

Josephson diode effect in topological superconductor

Zhaochen Liu,^{1,2} Linghao Huang,^{1,2} and Jing Wang^{1,2,3,4,*}

¹State Key Laboratory of Surface Physics and Department of Physics, Fudan University, Shanghai 200433, China

²Shanghai Research Center for Quantum Sciences, Shanghai 201315, China

³Institute for Nanoelectronic Devices and Quantum Computing, Fudan University, Shanghai 200433, China

⁴Hefei National Laboratory, Hefei 230088, China

We investigate the Josephson diode effect (JDE) in topological Josephson junctions. By both analytic and numerical calculations, we find that while a Josephson junction in the topological phase may exhibit higher diode efficiency compared to that in the trivial phase, this behavior is not universal. The presence of Majorana bound states is not a sufficient condition for a large diode effect. Furthermore, the diode efficiency undergoes substantial changes only in *specific* regions along the topological phase transition boundary, and a significant diode effect does coincide with the topological phases. Thereby our paper suggests the utilization of topological superconductivity for enhanced JDE, and also the Josephson diode effect may serve as an indicator for topological superconductor phase. These results suggest a nuanced relationship between the topological aspects of Josephson junctions and Josephson diode effect.

I. INTRODUCTION

Superconductivity, a fascinating macroscopic quantum phenomenon with profound physical significance and diverse practical applications, has been the focus of extensive research for decades [1]. In recent years, the burgeoning field of topological superconductivity has emerged as an exciting frontier in condensed matter physics [2–6]. Topological superconductors are predicted to host exotic quasiparticles, Majorana bound states (MBS) [7–9], which are topologically protected and exhibit non-Abelian exchange statistics [10], and have potential applications in topological quantum computation [11–13]. One of the most promising avenues for realizing topological superconductivity is through the Josephson junctions [14–19], which are composed of two superconductors interconnected by a weak-link. When a junction is expected to transition into a topological superconducting phase, unpaired MBS will emerge at the junction interfaces. So far substantial theoretical studies have investigated the exotic properties that MBS may exhibit in the topological Josephson junctions [3, 20–35].

Recently, a diode effect has been proposed and discovered in Josephson junctions, termed as the Josephson diode effect (JDE) [36–45]. A Josephson diode has asymmetric critical currents in the forward (I_c^+) and backward (I_c^-) directions [46]. Therefore, it manifests superconductive in one direction while resistive in the other direction when the magnitude of current falls within the range $\min\{I_c^-, I_c^+\} < I < \max\{I_c^-, I_c^+\}$. In comparison to superconducting diode effect in bulk systems [47–56], Josephson junctions may attain higher diode efficiency due to the suppression of kinetic energy, and thereby the enhancement of the influence of interactions [57]. Additionally, the supercurrent within a Josephson junction can be more controllable by adjusting the phase differ-

ence between the two superconductors [58], facilitating a deeper understanding of the underlying mechanism in diode effect.

Since the appearance of MBS in topological superconductors induces alterations in the energy spectrum of Josephson junctions, it further modifies the current-phase relation. This prompts the consideration of the potential impact of MBS on the JDE. However up to date, there is less focus on the feature of JDE in the presence of MBS [57, 59–65]. These studies provide some insights into the relationship between diode effect and topological phase transitions, but the influence of MBS on JDE as well as the relation between topological superconductors and JDE still needs more investigations.

Here we study the JDE in two representative systems consisting of topological superconductors. Specifically, we consider a proximitized semiconducting nanowire with strong Rashba spin-orbital coupling (SOC), and a two-dimensional magnetic topological insulator (TI) thin film proximity coupled to *s*-wave superconductivity. By employing the Bogoliubov-de Gennes (BdG) mean-field calculation, we find that the presence of MBS in the topological phase strongly affects the asymmetry of the Andreev spectrum, which leads to JDE. Moreover, the topological phase can exhibit higher diode efficiency compared to the trivial phase under certain conditions, specifically the diode efficiency undergoes substantial changes only in specific regions along the topological phase transition boundary, and a significant diode effect does coincide with the topological phases. Our paper suggests the utilization of topological superconductivity for enhanced JDE, while it also suggests JDE may serve as an indicator for topological superconductors in experiments.

* wjingphys@fudan.edu.cn

II. RASHBA NANOWIRE

A. Model

We start from a paradigmatic system of Josephson junctions: a Rashba nanowire with proximity-induced pairing correlation, see Fig. 1(a). The BdG Hamiltonian for this system is given by [15, 16]

$$\hat{H}_{1d} = \frac{1}{2} \int dx \hat{\Psi}^\dagger(x) \mathcal{H}_{1d} \hat{\Psi}(x) \quad (1)$$

with $\hat{\Psi}(x) \equiv (\psi_\uparrow, \psi_\downarrow, \psi_\uparrow^\dagger, \psi_\downarrow^\dagger)^T$, and

$$\mathcal{H}_{1d} = \left(\frac{k^2}{2m} - \mu + m_z \sigma_z \right) \tau_z + m_y \sigma_y + \alpha k \sigma_y \tau_z + \Delta(x),$$

where $k \equiv -i\hbar\partial_x$, the Zeeman coupling m_y and m_z are induced by the external magnetic field, μ is the chemical potential, α is the SOC strength and $\Delta(x)$ is the s -wave pairing potential. σ_i and τ_i ($i = x, y, z$) are Pauli matrices for spin and Nambu space, respectively. For the Josephson junction with phase difference ϕ between two superconductors, the pairing is $\Delta(x) = \Delta \sigma_y \tau_y$ for $x \leq 0$ and $\Delta(x) = \Delta e^{i\phi} \sigma_y (\tau_y - i\tau_x)/2 + \text{h.c.}$ for $x > L$, with L as the length of the junction. We focus on the experimentally important case of short junction.

In general, the Josephson current can be divided into two parts: one comes from the Andreev bound states (ABS) and the other is contributed from the continuum states [38, 62, 66]. The Josephson current is related to the spectrum of \mathcal{H}_{1d} by [67]

$$I(\phi) = \frac{2e}{\hbar} \frac{\partial E}{\partial \phi}, \quad E = -\frac{1}{2} \sum_{E_n \geq 0} E_n(\phi), \quad (2)$$

where the summation includes both the ABS and continuum states. Hereafter, we set $e = 1$ and $\hbar = 1$.

B. Symmetry analysis

Before explicit calculation, we first analyze the role of symmetries on the critical current I_c^\pm [39, 40, 52], denoting the maximum amplitude of the Josephson current for forward and backward directions, respectively. Without loss of generality, we assume that the Josephson current flows along the x axis, then the operations of time reversal (\mathcal{T}), mirror reflection with respect to the x axis (\mathcal{M}_x), and space inversion (\mathcal{P}) can reverse the current direction, whereas the other two mirror reflection operations (\mathcal{M}_y and \mathcal{M}_z) can not. Taking \mathcal{T} as an example, if a system exhibits \mathcal{T} symmetry when no Josephson current flows across the junction (with its Hamiltonian denoted as $H(0)$), then the system with forward current $H(I_0\hat{x})$ is related to the system with backward current $H(-I_0\hat{x})$ via \mathcal{T} operation. Therefore, the forward and backward critical current are equal: $I_c^+ = I_c^-$, indicating the absence of a diode effect. Similarly, \mathcal{M}_x (\mathcal{P}) also

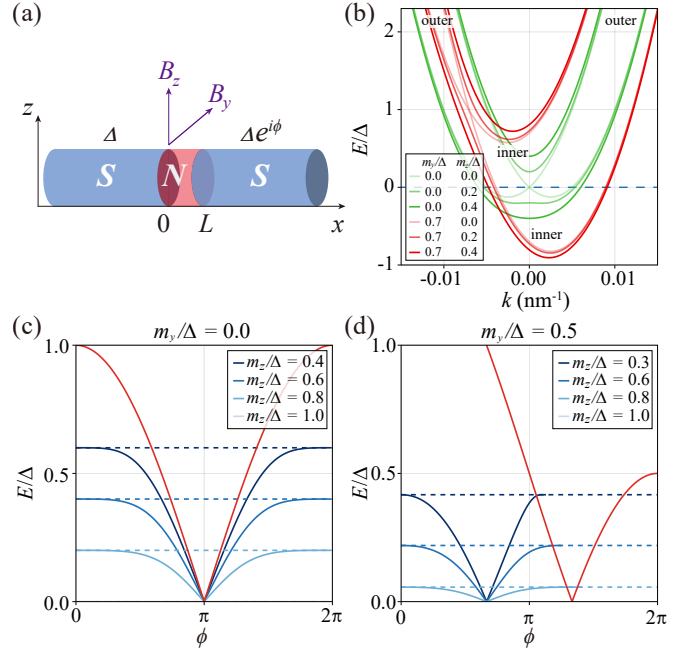


FIG. 1. (a) Sketch of a Josephson junction along the x -axis with normal state region of finite length L . The SOC is along the y -axis and external magnetic field has both y and z components. (b) Band structure of normal state in Rashba nanowire. m_z term opens an energy gap while m_y asymmetrizes the band structure. The system consists of a pair of outer modes and a pair of inner modes, and the induced s -wave superconducting pairing acts within each pair of modes. (c) and (d) The ABS spectrum with respect to different m_z for $m_y/\Delta = 0$ and $m_y/\Delta = 0.5$, respectively. The red (blue) lines are spectrum of outer (inner) modes, and the dashed lines mark the upper bound energy for inner modes.

ensure $I_c^+ = I_c^-$. Conversely, \mathcal{M}_y and \mathcal{M}_z symmetries impose no constraints on I_c^\pm . Hence symmetries like \mathcal{T} , \mathcal{M}_x , \mathcal{P} , or combined symmetries such as $\mathcal{T}\mathcal{M}_y$, $\mathcal{T}\mathcal{M}_z$, $\mathcal{M}_x\mathcal{M}_y$, $\mathcal{M}_x\mathcal{M}_z$, $\mathcal{P}\mathcal{M}_y$, $\mathcal{P}\mathcal{M}_z$ and $\mathcal{T}\mathcal{M}_y\mathcal{M}_z$ can enforce the vanishing of JDE. In the system under consideration, $\mathcal{T} = -i\sigma_y\mathcal{K}$ where \mathcal{K} is complex conjugate, $\mathcal{M}_x = \sigma_x$, $\mathcal{M}_y = \sigma_y$, $\mathcal{M}_z = \sigma_z$ and $\mathcal{P} = \sigma_0\tau_0$. The \mathcal{P} symmetry requires $\mathcal{P}H(k)\mathcal{P}^{-1} = H(-k)$, which has been broken by the SOC term, $\alpha k \sigma_y \tau_z$. Without the Zeeman term, the system exhibits \mathcal{T} , \mathcal{M}_x , $\mathcal{T}\mathcal{M}_y$, $\mathcal{M}_x\mathcal{M}_y$ and $\mathcal{P}\mathcal{M}_z$ symmetries, thus has no diode effect. If $m_z \neq 0$ and $m_y = 0$, \mathcal{T} and \mathcal{M}_x are broken but there remain $\mathcal{T}\mathcal{M}_y$, $\mathcal{M}_x\mathcal{M}_y$ and $\mathcal{P}\mathcal{M}_z$, giving rise to a zero diode effect. For $m_z = 0$ and $m_y \neq 0$, all of the above symmetries are broken. However, there is a hidden symmetry with $U(x)\mathcal{P}U(x)^\dagger$, where $U(x) = \exp(-i\alpha m_x \sigma_y/2)$ is the spin twist operator [39]. $U(x)$ eliminates SOC, and \mathcal{P} symmetry requires $I_c^+ = I_c^-$. Therefore, to obtain JDE, both the Zeeman terms m_y and m_z are necessary.

As a side note, in this system, zero supercurrent is reached at $\phi = 0$. If an anomalous phase shift occurs, zero supercurrent will arise at a finite phase difference $\phi = \phi_0$. Therefore, the symmetry analysis should be done

at $\phi - \phi_0 = 0$, and the property of ϕ_0 under symmetry transformations should be considered in the symmetry analysis. However, the symmetry requirement itself does not change; all the symmetries mentioned above should still be broken.

C. Results

In what follows, we discuss the JDE and topological phase transition in this system by analyzing the Andreev spectrum. The ABS can be determined using the wave function matching condition in the short junction limit (i.e., junction length $L \ll \xi$ superconducting coherence length). For simplicity of analytical calculation, we first consider the short junction limit with $L = 0$ and choose $\mu = 0$. Assuming that SOC dominates $m\alpha^2 \gg \Delta, m_y, m_z$, then the linearized Hamiltonian for the low-energy physics of inner and outer modes [Fig. 1(b)] can be obtained near $k_{\text{in}} = 0$ and $k_{\text{out}} = \pm 2m\alpha$, respectively [63, 68]

$$\begin{aligned} H_{\text{in}} &= \alpha k \sigma_y \tau_z + m_z \sigma_z \tau_z + m_y \sigma_y \tau_0 + \Delta(x), \\ H_{\text{out}} &= -\alpha k \sigma_y \tau_z + m_y \sigma_y \tau_0 + \Delta(x). \end{aligned} \quad (3)$$

For H_{out} , $\sigma_y = \mp$ corresponds to $k_{\text{out}} = \pm 2m\alpha$ modes. We assume that the inter-mode scattering at the junction interface is neglected, and thus treat different modes independently. The Hamiltonian with $m_z = 0$ resembles previous results on the finite momentum pairing [38], which can be seen from the gauge transformation $\psi(x) \rightarrow \exp(\mp i m_y x / \alpha) \tau_z \psi(x)$ for inner and outer modes, respectively. Then the m_y term is eliminated, while the pairing term carries an additional phase factor $e^{\mp i 2 m_y x / \alpha}$, which means Cooper pairs in two modes get opposite momentum. Then the Andreev spectrum of outer modes are

$$E_1^{\text{out}} = \Delta \cos(\phi/2) + m_y, E_2^{\text{out}} = -\Delta \cos(\phi/2) - m_y. \quad (4)$$

The current-phase relation is obtained from Eq. (2) as $I_{\text{out}} = \Delta \sin(\phi/2) \text{sgn}(\Delta \cos(\phi/2) + m_y)/2$. Thus the contribution from ABS to JDE is $I_c^+ - I_c^- = \text{sgn}(m_y) \Delta (1 - \sqrt{1 - (m_y/\Delta)^2})/2$. For inner modes, when $m_z = 0$, the spectrum is exactly symmetric to the outer modes, which can be seen from the corresponding Hamiltonian and Andreev spectrum

$$E_1^{\text{in}} = \Delta \cos(\phi/2) - m_y, E_2^{\text{in}} = -\Delta \cos(\phi/2) + m_y. \quad (5)$$

This means the contributions of two modes exactly compensate each other. Besides, the Josephson current created by continuum states is independent of ϕ [38]. As a consequence, no JDE occurs, which is consistent with the previous symmetry analysis.

Including nonzero m_z does not influence the outer modes, yet the inner modes are no longer symmetric to the outer ones. The corresponding equations become too complicated for analytical solution with nonzero m_z and m_y , we solve the spectrum numerically. As shown in

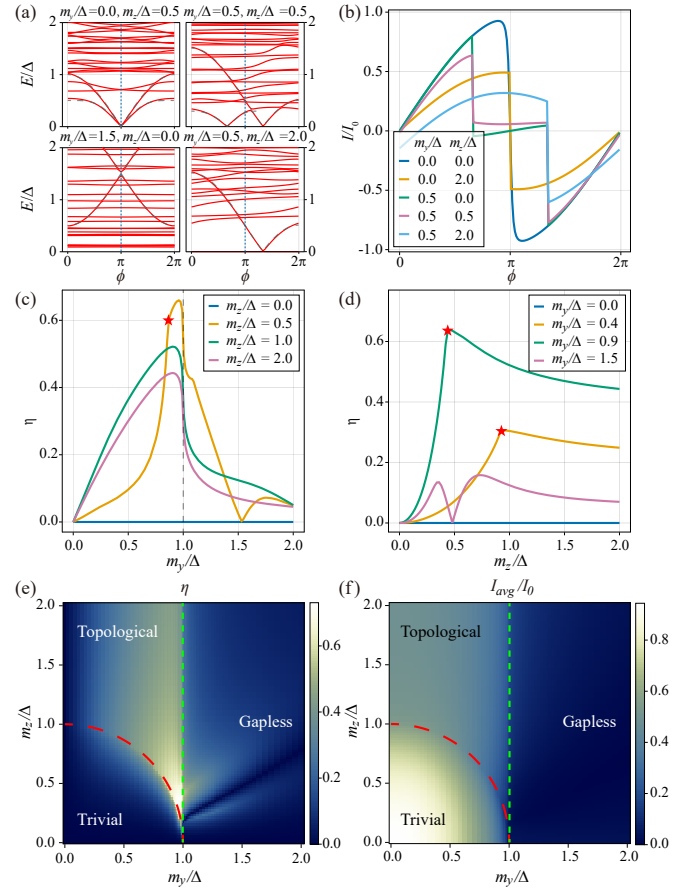


FIG. 2. (a) Energy spectrum of one-dimensional short junction near Fermi energy with respect to ϕ at different (m_y, m_z) . The dashed lines are the analytical results in Eq. (4). (b) Current-phase relation. (c) η vs m_y for typical m_z . For $m_z/\Delta < 1$, the star symbol marks the boundary between topological and trivial gapped phases. (d) η vs m_z for several m_y . The star symbol marks the phase boundary when $m_y/\Delta < 1$. (e) and (f) The dependence of η and I_{avg} on (m_y, m_z) , where $I_0 \equiv e\Delta/\hbar$. The red dashed lines indicate the phase boundary. The green dashed lines delineate the boundary between gapped and gapless regions.

Figs. 1(c) and 1(d), the spectrum is symmetric about $\phi = \pi$ when $m_y \neq 0, m_z = 0$. With nonzero m_z , the inner modes get suppressed, and their contribution to Josephson current would no longer compensate for the outer ones. Thus the imbalance between these two modes generates nonzero JDE. It is expected that the efficiency factor of JDE, $\eta \equiv (|I_c^+ - I_c^-|)/(I_c^+ + I_c^-)$, increases as m_z approaches the topological phase boundary due to further suppression of the inner modes. Furthermore, we notice that the inner modes are upper bounded by $\Delta - \sqrt{m_z^2 + m_y^2}$, so they disappear after the topological transition for $m_z^2 + m_y^2 > \Delta^2$ and only the outer modes solely contribute to the Josephson current.

The topology comes from the single Fermi surface condition. In the trivial region, two band inversions occur at

the inner and outer Fermi points. While for the topological region, only the band inversion at the outer ones remains. On the other hand, the diode effect is suppressed due to the compensation of these two modes. Thus, coincidence of these two different phenomena could be expected. However, as we can see in the numerical results below, this does not mean that topology is a *sufficient* condition for a large diode effect.

As studied previously, the contribution from the continuum states is important for determining the magnitude of the asymmetry between the critical currents in opposite directions [38]. In Fig. 2, we numerically calculate the low-energy spectrum, the diode efficiency factor η , and current-phase relation by taking the contribution from continuum of states into account. We discretize Eq. (1) on the lattice, and set $\Delta = 1$ meV, $\alpha = 100$ meV·nm, $m = 2.5 \times 10^{-3}$ nm⁻²·meV⁻¹, $a = 10$ Å, and $L = 2a$. Here $m\alpha^2/\Delta = 25$ ensures that SOC dominates over superconducting pairing and Zeeman field. We set the total length of nanowire as $1000a$. To get rid of finite size effects, the total DC Josephson current and diode efficiency η are calculated by the Green's function method [69, 70]. The low-energy spectrum is plotted in Fig. 2(a), where the dashed lines represent the analytical results for the ABS spectrum, which match well with the numerical results. When $m_y = 0$, the spectrum is symmetric with respect to $\phi = \pi$, and a similar situation also occurs for $m_z = 0$. Only if both m_y and m_z are nonzero, the spectrum can be asymmetric, giving rise to JDE. The current-phase relation for several typical parameters is shown in Fig. 2(b). The discontinuity in the current-phase relation is due to the ABS changing direction at corresponding points.

To better understand JDE, we calculate the evolution of η versus (m_y, m_z) . For fixed $m_z \neq 0$ shown in Fig. 2(c), η increases as m_y approaches the phase boundary from trivial side, which accounts for the suppression of ABS from inner modes. When $m_z/\Delta \geq 1$, the system is in the topological phase for $m_y < \Delta$ and η first increases, and then it enters into gapless phase for $m_y \geq \Delta$ with η dramatically decreasing. The m_y term is regarded as the momentum of Cooper pairs under the gauge transformation. Therefore, when $m_y/\Delta < 1$, the Doppler shift in energy becomes larger as m_y increases, and the asymmetry between the critical currents becomes larger, resulting in higher η . The region $m_y/\Delta \geq 1$ corresponds to gapless superconductivity, where quasiparticles at zero-energy exist and introduce complexity into the behavior of the Josephson current, and η shows nonmonotonic dependence on m_z . For fixed nonzero m_y in Fig. 2(d), η grows as m_z increases before the phase transition, also resulting from the suppression of inner modes. η exhibits a crossover from the trivial to the topological phase. After the phase transition, only outer modes of ABS contribute to Josephson current, and η decreases slowly in m_z . Interestingly, η has a *kink* at the phase boundary between topological and trivial gapped superconductor.

The dependence of η and the averaged critical current

$I_{\text{avg}} = |I_c^+ + I_c^-|$ on (m_y, m_z) are shown in Figs. 2(e) and 2(f), respectively. We can see that η changes significantly along $m_y/\Delta = 1$ and part of the phase transition boundary, then JDE seems to be a *weak indicator* for topological phase transition. I_{avg} decreases to be a small value when $m_y > \Delta$, where the critical current I_c^\pm is also small, thus JDE in this region has little practical significance. We emphasize that in this model, η is continuous but has a kink near the topological phase transition. Thus when (m_y, m_z) are slightly smaller than its critical value for the topological transition, a large η can be still reached, where no MBS exists. On the other hand, not all the topological region in Fig. 2(e) exhibits a large η . These observations suggest that the emergence of MBS may not be the essential factor for enhancing JDE, at least not always. Moreover, when m_y is small, η changes little as m_z increases, indicating that in this region, the topological phase transition does not have a significant impact on η .

III. MAGNETIC TI HETEROSTRUCTURE

Now we study JDE in 2D topological superconductivity, which consists of a magnetic TI thin film proximity coupled to an *s*-wave superconductor [71–73]. The BdG Hamiltonian is described by two surface Dirac fermions with superconducting pairing,

$$\mathcal{H}_{2d} = \begin{pmatrix} \mathcal{H}_0(\mathbf{k}) & \Delta \\ \Delta^\dagger & -\mathcal{H}_0^*(-\mathbf{k}) \end{pmatrix}, \quad (6)$$

where $\mathcal{H}_0(\mathbf{k}) = v(k_y\sigma_x - k_x\sigma_y)\xi_z + m(\mathbf{k})\xi_x + \mathbf{m} \cdot \boldsymbol{\sigma} - \mu$, $\Delta = \Delta(x, y)(\xi_0 + \xi_z)/2$ is the superconducting pairing induced on the top layer with $\Delta(x, y) = \Delta(x)$. We consider the planar Josephson junction [74–77] with $\Delta(x) = i\Delta\sigma_y$ for $x \leq 0$ and $\Delta(x) = i\Delta e^{i\phi}\sigma_y$ for $x > L$. σ_i and ξ_i ($i = x, y, z$) are Pauli matrices for spin and layer, respectively. v is Dirac velocity, $m(\mathbf{k}) = m_0 + m_1(k_x^2 + k_y^2)$ represents the interlayer coupling, \mathbf{m} is the Zeeman term, and μ is the chemical potential. We focus on the short junction.

We then analyze the symmetry constraints of JDE in this system. Without the Zeeman and pairing terms, the system has time-reversal symmetry $\mathcal{T} = -i\sigma_y\mathcal{K}$, mirror symmetries $\mathcal{M}_x = \sigma_x$, $\mathcal{M}_y = \sigma_y$, $\mathcal{M}_z = \sigma_z\xi_x$ and inversion symmetry $\mathcal{P} = \xi_x$. To obtain a nonzero JDE with Josephson current along the *x*-direction, we need to break symmetries such as \mathcal{T} , \mathcal{M}_x , \mathcal{P} , $\mathcal{T}\mathcal{M}_y$, $\mathcal{T}\mathcal{M}_z$, $\mathcal{M}_x\mathcal{M}_y$, $\mathcal{M}_x\mathcal{M}_z$, $\mathcal{P}\mathcal{M}_y$, $\mathcal{P}\mathcal{M}_z$ and $\mathcal{T}\mathcal{M}_y\mathcal{M}_z$. Therefore, an asymmetric pairing term is introduced to break \mathcal{P} , $\mathcal{T}\mathcal{M}_z$, $\mathcal{M}_x\mathcal{M}_z$ and $\mathcal{P}\mathcal{M}_y$. The other symmetries are broken by the Zeeman term m_y . Here we consider the external magnetic field is applied along both the *y* and *z* axis.

The phase diagram of underlying system has been studied previously [71], where the phase boundaries are determined by the bulk BdG gap closing at $\mathbf{k} = 0$. For $m_y = 0$ and $\mu = 0$, the phase boundary is given

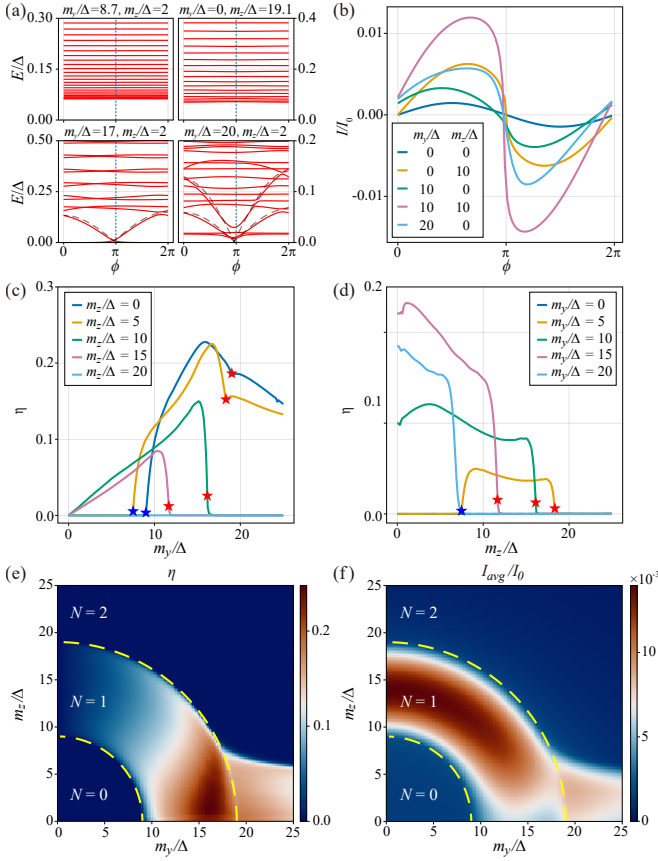


FIG. 3. (a) Energy spectrum of 2D magnetic TI heterostructure near Fermi energy with respect to ϕ at different (m_y, m_z) . (b) Current-phase relation. (c) η vs m_y . (d) η vs m_z . The blue star symbol marks the phase boundary between trivial and $N = 1$ phase, and the red marks boundary between $N = 1$ and $N = 2$ phase. (e) and (f) η and I_{avg} vs (m_y, m_z) , respectively. The dashed yellow lines indicate the phase boundary.

by $\pm\Delta m_z + m_z^2 = m_0^2$. Each gapped phase is characterized by a BdG Chern number N . $N = 0$ for $|m_z| < (\sqrt{\Delta^2 + 4m_0^2} - \Delta)/2$, $N = \text{sgn}(m_z)$ when $(\sqrt{\Delta^2 + 4m_0^2} - \Delta)/2 < |m_z| < (\sqrt{\Delta^2 + 4m_0^2} + \Delta)/2$, and $N = 2\text{sgn}(m_z)$ for $|m_z| > (\sqrt{\Delta^2 + 4m_0^2} + \Delta)/2$. When $m_y \neq 0$ and $\mu \neq 0$, the phase diagram is obtained through adiabatic evolution to that when $m_y = 0$ and $\mu = 0$. The $N = 0$ and $N = 2$ phases are adiabatically connected to trivial insulator and quantum anomalous Hall insulator without gap closure, respectively. $N = 1$ phase is the nontrivial topological superconductor which has a single chiral Majorana edge mode, and we will see below the influence of topology on JDE.

We numerically calculate JDE in Fig. 3, and set $m_0 = -14$ meV, $a = 20$ Å, $v = 3.2$ eV·Å, $m_1 = 9.405$ eV·Å², $\Delta = 1$ meV, $L = 2a$. Furthermore, we set $\mu = 5$ meV since a finite chemical potential would enhance the proximity effect and enlarge $N = 1$ phase [71, 78]. With periodic boundary condition along the y -axis, the Josephson current can be expressed as $I(\phi) = \int dk_y/2\pi I(k_y, \phi)$.

In Fig. 3(a), we present the low-energy spectrum of the planar Josephson junction at $k_y = 0$ for typical parameters, where the junction length in the x -direction is set as $5000a$. For $m_y = 0$, the spectrum is symmetric with respect to $\phi = \pi$ [14, 79]. The introduction of a nonzero m_y leads to an asymmetry in the bound state spectrum. Moreover, when the Zeeman term predominantly lies in the x - y plane [second row of Fig. 3(a)], there is a clear imbalance between the two branches, and their dispersion can be fitted into Eq. (4). Then JDE is expected. However, for regions where either the interlayer hybridization or Zeeman terms dominates [first row of Fig. 3(a)], the system does not develop superconducting correlation and the ABS is absent, resulting in a vanishing JDE. The η vs m_y and m_z are plotted in Figs. 3(c) and 3(d), respectively. It is evident that when $m_z/\Delta < 9$ is small, the system undergoes two topological phase transitions as m_y increases. JDE almost vanishes in the $N = 0$ phase. In contrast, both $N = 1$ and $N = 2$ phases manifest finite η . When the system is deep inside the $N = 2$ phase, η almost vanishes for the Zeeman terms dominate.

In Figs. 3(e) and 3(f), we present η and I_{avg} as functions of (m_y, m_z) . Here I_{avg} serves as an indicator of the dominance of superconducting correlation. Thus η only has a nonzero value within the region where $I_{\text{avg}} \neq 0$. Similar to the nanowire case, η changes significantly along part of the phase boundary, and not all the topological region exhibits a large η . However, the largest η resides in the topological $N = 1$ phase. With combined η and I_{avg} , we can identify large part of $N = 1$ phase by JDE, namely large JDE is an indicator for $N = 1$ topological phase. However, the identification of the phase boundary by JDE is not obvious.

IV. CONCLUSION

We have analyzed the JDE in two representative models consisting of topological superconductors in one and two dimensions. Our results indicate that, in general, the diode efficiency can be high but not always in the topological phase. A Josephson junction in the trivial phase can also achieve relative high diode efficiency. This suggests that the existence of MBS is not a sufficient condition for realizing a large JDE. On the other hand, a significant diode effect does coincide with the topological phases, and the distinct change in diode efficiency occurs alongside some segments of the topological phase transition boundaries. In this sense, JDE with combined η and I_{avg} can serve as an indicator for topological superconductor phase. We hope the theoretical work here could aid the identification of topological superconductivity by using JDE.

ACKNOWLEDGMENTS

This work is supported by the National Key Research Program of China under Grant No. 2019YFA0308404, the Natural Science Foundation of China through Grants No. 12350404 and No. 12174066, the Innovation Program for Quantum Science and Technology through

Grant No. 2021ZD0302600, the Science and Technology Commission of Shanghai Municipality under Grant No. 23JC1400600, Shanghai Municipal Science and Technology Major Project under Grant No. 2019SHZDZX01.

Note added: During the preparation of our manuscript, we learned of an independent work on a similar problem [80]. However, their model and conclusion are different from our results.

-
- [1] M. Tinkham, *Introduction to Superconductivity, 2nd Edition* (Dover Publications, 2004).
 - [2] X.-L. Qi and S.-C. Zhang, Topological insulators and superconductors, *Rev. Mod. Phys.* **83**, 1057 (2011).
 - [3] Y. Tanaka, M. Sato, and N. Nagaosa, Symmetry and topology in superconductors –odd-frequency pairing and edge states–, *J. Phys. Soc. Jpn.* **81**, 011013 (2012).
 - [4] Y. Ando and L. Fu, Topological crystalline insulators and topological superconductors: From concepts to materials, *Annu. Rev. Condens. Matter Phys.* **6**, 361 (2015).
 - [5] C.-K. Chiu, J. C. Y. Teo, A. P. Schnyder, and S. Ryu, Classification of topological quantum matter with symmetries, *Rev. Mod. Phys.* **88**, 035005 (2016).
 - [6] M. Sato and Y. Ando, Topological superconductors: a review, *Rep. Prog. Phys.* **80**, 076501 (2017).
 - [7] A. Y. Kitaev, Unpaired majorana fermions in quantum wires, *Phys.-Usp.* **44**, 131 (2001).
 - [8] M. Leijnse and K. Flensberg, Introduction to topological superconductivity and majorana fermions, *Semicond. Sci. Technol.* **27**, 124003 (2012).
 - [9] C. Beenakker, Search for majorana fermions in superconductors, *Annu. Rev. Condens. Matter Phys.* **4**, 113 (2013).
 - [10] D. A. Ivanov, Non-abelian statistics of half-quantum vortices in p -wave superconductors, *Phys. Rev. Lett.* **86**, 268 (2001).
 - [11] A. Y. Kitaev, Fault-tolerant quantum computation by anyons, *Ann. Phys.* **303**, 2 (2003).
 - [12] C. Nayak, S. H. Simon, A. Stern, M. Freedman, and S. Das Sarma, Non-abelian anyons and topological quantum computation, *Rev. Mod. Phys.* **80**, 1083 (2008).
 - [13] D. Aasen, M. Hell, R. V. Mishmash, A. Higginbotham, J. Danon, M. Leijnse, T. S. Jespersen, J. A. Folk, C. M. Marcus, K. Flensberg, and J. Alicea, Milestones toward majorana-based quantum computing, *Phys. Rev. X* **6**, 031016 (2016).
 - [14] L. Fu and C. L. Kane, Superconducting proximity effect and majorana fermions at the surface of a topological insulator, *Phys. Rev. Lett.* **100**, 096407 (2008).
 - [15] R. M. Lutchyn, J. D. Sau, and S. Das Sarma, Majorana fermions and a topological phase transition in semiconductor-superconductor heterostructures, *Phys. Rev. Lett.* **105**, 077001 (2010).
 - [16] Y. Oreg, G. Refael, and F. von Oppen, Helical liquids and majorana bound states in quantum wires, *Phys. Rev. Lett.* **105**, 177002 (2010).
 - [17] J. Alicea, Majorana fermions in a tunable semiconductor device, *Phys. Rev. B* **81**, 125318 (2010).
 - [18] M. Hell, M. Leijnse, and K. Flensberg, Two-dimensional platform for networks of majorana bound states, *Phys. Rev. Lett.* **118**, 107701 (2017).
 - [19] F. Pientka, A. Keselman, E. Berg, A. Yacoby, A. Stern, and B. I. Halperin, Topological superconductivity in a planar josephson junction, *Phys. Rev. X* **7**, 021032 (2017).
 - [20] Y. Tanaka and S. Kashiwaya, Theory of the josephson effect in d -wave superconductors, *Phys. Rev. B* **53**, R11957 (1996).
 - [21] Y. Tanaka and S. Kashiwaya, Theory of josephson effects in anisotropic superconductors, *Phys. Rev. B* **56**, 892 (1997).
 - [22] Y. Tanaka, T. Yokoyama, and N. Nagaosa, Manipulation of the majorana fermion, andreev reflection, and josephson current on topological insulators, *Phys. Rev. Lett.* **103**, 107002 (2009).
 - [23] Y. Tanaka, Y. Mizuno, T. Yokoyama, K. Yada, and M. Sato, Anomalous andreev bound state in noncentrosymmetric superconductors, *Phys. Rev. Lett.* **105**, 097002 (2010).
 - [24] P. San-Jose, E. Prada, and R. Aguado, ac josephson effect in finite-length nanowire junctions with majorana modes, *Phys. Rev. Lett.* **108**, 257001 (2012).
 - [25] J. Cayao, E. Prada, P. San-Jose, and R. Aguado, Sns junctions in nanowires with spin-orbit coupling: Role of confinement and helicity on the subgap spectrum, *Phys. Rev. B* **91**, 024514 (2015).
 - [26] F. Dolcini, M. Houzet, and J. S. Meyer, Topological josephson ϕ_0 junctions, *Phys. Rev. B* **92**, 035428 (2015).
 - [27] Y. Peng, F. Pientka, E. Berg, Y. Oreg, and F. von Oppen, Signatures of topological josephson junctions, *Phys. Rev. B* **94**, 085409 (2016).
 - [28] J. Cayao, P. San-Jose, A. M. Black-Schaffer, R. Aguado, and E. Prada, Majorana splitting from critical currents in josephson junctions, *Phys. Rev. B* **96**, 205425 (2017).
 - [29] J. Cayao, A. M. Black-Schaffer, E. Prada, and R. Aguado, Andreev spectrum and supercurrents in nanowire-based sns junctions containing majorana bound states, *Beilstein J. Nanotechnol.* **9**, 1339 (2018).
 - [30] C.-Z. Chen, J. J. He, M. N. Ali, G.-H. Lee, K. C. Fong, and K. T. Law, Asymmetric josephson effect in inversion symmetry breaking topological materials, *Phys. Rev. B* **98**, 075430 (2018).
 - [31] Y. Tokura and N. Nagaosa, Nonreciprocal responses from non-centrosymmetric quantum materials, *Nat Commun* **9**, 3740 (2018).
 - [32] J. Cayao and A. M. Black-Schaffer, Distinguishing trivial and topological zero-energy states in long nanowire junctions, *Phys. Rev. B* **104**, L020501 (2021).
 - [33] L. Baldo, L. G. G. V. D. D. Silva, A. M. Black-Schaffer, and J. Cayao, Zero-frequency supercurrent susceptibility signatures of trivial and topological zero-energy states in nanowire junctions, *Supercond. Sci. Technol.* **36**, 034003 (2023).

- (2023).
- [34] M. C. Dartailh, W. Mayer, J. Yuan, K. S. Wickramasinghe, A. Matos-Abiague, I. Žutić, and J. Shabani, Phase signature of topological transition in josephson junctions, *Phys. Rev. Lett.* **126**, 036802 (2021).
 - [35] Y. Tanaka and S. Tamura, Theory of surface andreev bound states and odd-frequency pairing in superconductor junctions, *J. Supercond. Nov. Magn.* **34**, 1677 (2021).
 - [36] J. Hu, C. Wu, and X. Dai, Proposed design of a josephson diode, *Phys. Rev. Lett.* **99**, 067004 (2007).
 - [37] K. Misaki and N. Nagaosa, Theory of the nonreciprocal josephson effect, *Phys. Rev. B* **103**, 245302 (2021).
 - [38] M. Davydova, S. Prembabu, and L. Fu, Universal josephson diode effect, *Sci. Adv.* **8**, eabo0309 (2022).
 - [39] D. Wang, Q.-H. Wang, and C. Wu, Symmetry constraints on direct-current josephson diodes (2022), [arxiv:2209.12646 \[cond-mat\]](https://arxiv.org/abs/2209.12646).
 - [40] Y. Zhang, Y. Gu, P. Li, J. Hu, and K. Jiang, General theory of josephson diodes, *Phys. Rev. X* **12**, 041013 (2022).
 - [41] C. Baumgartner, L. Fuchs, A. Costa, S. Reinhardt, S. Gronin, G. C. Gardner, T. Lindemann, M. J. Manfra, P. E. Faria Junior, D. Kochan, J. Fabian, N. Paradiso, and C. Strunk, Supercurrent rectification and magnetochiral effects in symmetric josephson junctions, *Nat. Nanotechnol.* **17**, 39 (2022).
 - [42] H. Wu, Y. Wang, Y. Xu, P. K. Sivakumar, C. Pasco, U. Filippozzi, S. S. P. Parkin, Y.-J. Zeng, T. McQueen, and M. N. Ali, The field-free josephson diode in a van der waals heterostructure, *Nature* **604**, 653 (2022).
 - [43] B. Pal, A. Chakraborty, P. K. Sivakumar, M. Davydova, A. K. Gopi, A. K. Pandeya, J. A. Krieger, Y. Zhang, M. Date, S. Ju, N. Yuan, N. B. M. Schröter, L. Fu, and S. S. P. Parkin, Josephson diode effect from cooper pair momentum in a topological semimetal, *Nat. Phys.* **18**, 1228 (2022).
 - [44] X.-J. Liu and A. M. Lobos, Manipulating majorana fermions in quantum nanowires with broken inversion symmetry, *Phys. Rev. B* **87**, 060504 (2013).
 - [45] N. Nagaosa and Y. Yanase, Nonreciprocal transport and optical phenomena in quantum materials, *Annu. Rev. Condens. Matter Phys.* **15**, 63 (2024).
 - [46] M. Nadeem, M. S. Fuhrer, and X. Wang, The superconducting diode effect, *Nat. Rev. Phys.* **5**, 558 (2023).
 - [47] N. F. Q. Yuan and L. Fu, Topological metals and finite-momentum superconductors, *Proc. Natl. Acad. Sci.* **118**, e2019063118 (2021).
 - [48] A. Daido, Y. Ikeda, and Y. Yanase, Intrinsic superconducting diode effect, *Phys. Rev. Lett.* **128**, 037001 (2022).
 - [49] N. F. Q. Yuan and L. Fu, Supercurrent diode effect and finite-momentum superconductors, *Proc. Natl. Acad. Sci. U.S.A.* **119**, e2119548119 (2022).
 - [50] J. J. He, Y. Tanaka, and N. Nagaosa, A phenomenological theory of superconductor diodes, *New J. Phys.* **24**, 053014 (2022).
 - [51] K. Takasan, S. Sumita, and Y. Yanase, Supercurrent-induced topological phase transitions, *Phys. Rev. B* **106**, 014508 (2022).
 - [52] B. Zinkl, K. Hamamoto, and M. Sigrist, Symmetry conditions for the superconducting diode effect in chiral superconductors, *Phys. Rev. Research* **4**, 033167 (2022).
 - [53] F. Ando, Y. Miyasaka, T. Li, J. Ishizuka, T. Arakawa, Y. Shiota, T. Moriyama, Y. Yanase, and T. Ono, Observation of superconducting diode effect, *Nature* **584**, 373 (2020).
 - [54] Y. Miyasaka, R. Kawarazaki, H. Narita, F. Ando, Y. Ikeda, R. Hisatomi, A. Daido, Y. Shiota, T. Moriyama, Y. Yanase, and T. Ono, Observation of nonreciprocal superconducting critical field, *Appl. Phys. Express* **14**, 073003 (2021).
 - [55] H. Narita, J. Ishizuka, R. Kawarazaki, D. Kan, Y. Shiota, T. Moriyama, Y. Shimakawa, A. V. Ognev, A. S. Samardak, Y. Yanase, and T. Ono, Field-free superconducting diode effect in noncentrosymmetric superconductor/ferromagnet multilayers, *Nat. Nanotechnol.* **17**, 823 (2022).
 - [56] Y. Hou, F. Nichele, H. Chi, A. Lodesani, Y. Wu, M. F. Ritter, D. Z. Haxell, M. Davydova, S. Ilić, O. Glezakou-Elbert, A. Varambally, F. S. Bergeret, A. Kamra, L. Fu, P. A. Lee, and J. S. Moodera, Ubiquitous superconducting diode effect in superconductor thin films, *Phys. Rev. Lett.* **131**, 027001 (2023).
 - [57] Y. Tanaka, B. Lu, and N. Nagaosa, Theory of giant diode effect in *d*-wave superconductor junctions on the surface of a topological insulator, *Phys. Rev. B* **106**, 214524 (2022).
 - [58] K. K. Likharev, Superconducting weak links, *Rev. Mod. Phys.* **51**, 101 (1979).
 - [59] K. N. Nesterov, M. Houzet, and J. S. Meyer, Anomalous josephson effect in semiconducting nanowires as a signature of the topologically nontrivial phase, *Phys. Rev. B* **93**, 174502 (2016).
 - [60] C. Spånslätt, Geometric josephson effects in chiral topological nanowires, *Phys. Rev. B* **98**, 054508 (2018).
 - [61] A. G. Kutlin and A. S. Mel'nikov, Geometry-dependent effects in majorana nanowires, *Phys. Rev. B* **101**, 045418 (2020).
 - [62] A. A. Kopasov, A. G. Kutlin, and A. S. Mel'nikov, Geometry controlled superconducting diode and anomalous josephson effect triggered by the topological phase transition in curved proximitized nanowires, *Phys. Rev. B* **103**, 144520 (2021).
 - [63] C. Murthy, V. D. Kurilovich, P. D. Kurilovich, B. van Heck, L. I. Glazman, and C. Nayak, Energy spectrum and current-phase relation of a nanowire josephson junction close to the topological transition, *Phys. Rev. B* **101**, 224501 (2020).
 - [64] H. F. Legg, K. Laubscher, D. Loss, and J. Klinovaja, Parity-protected superconducting diode effect in topological josephson junctions, *Phys. Rev. B* **108**, 214520 (2023).
 - [65] J. J. Cuzzo, W. Pan, J. Shabani, and E. Rossi, Microwave-tunable diode effect in asymmetric squids with topological josephson junctions, *Phys. Rev. Res.* **6**, 023011 (2024).
 - [66] P. San-Jose, J. Cayao, E. Prada, and R. Aguado, Multiple andreev reflection and critical current in topological superconducting nanowire junctions, *New J. Phys.* **15**, 075019 (2013).
 - [67] C. W. J. Beenakker, Universal limit of critical-current fluctuations in mesoscopic josephson junctions, *Phys. Rev. Lett.* **67**, 3836 (1991).
 - [68] B. van Heck, J. I. Värynen, and L. I. Glazman, Zeeman and spin-orbit effects in the andreev spectra of nanowire junctions, *Phys. Rev. B* **96**, 075404 (2017).
 - [69] A. Furusaki, Dc josephson effect in dirty sns junctions: Numerical study, *Phys. B: Condens. Matter* **203**, 214 (1994).

- [70] Y.-T. Zhang, Z. Hou, X. C. Xie, and Q.-F. Sun, Quantum perfect crossed andreev reflection in top-gated quantum anomalous hall insulator–superconductor junctions, *Phys. Rev. B* **95**, 245433 (2017).
- [71] J. Wang, Q. Zhou, B. Lian, and S.-C. Zhang, Chiral topological superconductor and half-integer conductance plateau from quantum anomalous hall plateau transition, *Phys. Rev. B* **92**, 064520 (2015).
- [72] J. Wang, Electrically tunable topological superconductivity and majorana fermions in two dimensions, *Phys. Rev. B* **94**, 214502 (2016).
- [73] J. J. He, T. Liang, Y. Tanaka, and N. Nagaosa, Platform of chiral majorana edge modes and its quantum transport phenomena, *Commun. Phys.* **2**, 149 (2019).
- [74] C.-Z. Chen, J. J. He, D.-H. Xu, and K. T. Law, Emergent josephson current of $n = 1$ chiral topological superconductor in quantum anomalous hall insulator/superconductor heterostructures, *Phys. Rev. B* **98**, 165439 (2018).
- [75] C.-A. Li, J. Li, and S.-Q. Shen, Majorana-josephson interferometer, *Phys. Rev. B* **99**, 100504 (2019).
- [76] S. Ikegaya, S. Tamura, D. Manske, and Y. Tanaka, Anomalous proximity effect of planar topological josephson junctions, *Phys. Rev. B* **102**, 140505 (2020).
- [77] B. Lu, S. Ikegaya, P. Buset, Y. Tanaka, and N. Nagaosa, Tunable josephson diode effect on the surface of topological insulators, *Phys. Rev. Lett.* **131**, 096001 (2023).
- [78] X.-L. Qi, T. L. Hughes, and S.-C. Zhang, Chiral topological superconductor from the quantum hall state, *Phys. Rev. B* **82**, 184516 (2010).
- [79] L. Fu and C. L. Kane, Josephson current and noise at a superconductor/quantum-spin-hall-insulator/superconductor junction, *Phys. Rev. B* **79**, 161408 (2009).
- [80] J. Cayao, N. Nagaosa, and Y. Tanaka, Enhancing the josephson diode effect with majorana bound states, *Phys. Rev. B* **109**, L081405 (2024).